DNA methylation profiling in nanochannels

Shuang Fang Lim, Alena Karpusenko, John J. Sakon, Joseph A. Hook, Tyra A. Lamar, and Robert Riehn[a)]
Department of Physics, North Carolina State University, Raleigh, North Carolina 27695, USA

(Received 29 April 2011; accepted 24 June 2011; published online 25 July 2011)

We report the profiling of the 5-methyl cytosine distribution within single genomic-sized DNA molecules at a gene-relevant resolution. This method linearizes and stretches DNA molecules by confinement to channels with a dimension of about $250 \times 200\ \text{nm}^2$. The methylation state is detected using fluorescently labeled methyl-CpG binding domain proteins (MBD), with high signal contrast and low background. DNA barcodes consisting of methylated and non-methylated segments are generated, with both short and long concatemers demonstrating spatially resolved MBD binding. The resolution of the technique is better than 10 kbp, and single-molecule read-lengths exceeding 140 kbp have been achieved. © *2011 American Institute of Physics*. [doi:10.1063/1.3613671]

I. INTRODUCTION

Epigenetic regulation is the inheritable modification of gene activity without influencing the underlying DNA sequence. Such regulation can occur through nucleosome positioning, histone modifications, and DNA methylation.[1,2] DNA 5-cytosine methylation is one of the most widely studied mechanisms influencing epigenetic gene regulation and is generally thought to suppress gene expression. A CpG pattern in which cytosines on both strands carry this modification can be maintained through DNA replication and thus cell division. CpG dinucleotides are clustered in the CpG islands (guanine-cytosine (GC) rich regions) that are present at the 5′ ends of about 40% of mammalian genes.[3] The methylation of CpG islands contributes to various biological processes such as parental genomic imprinting, X-chromosomal inactivation, cellular differentiation, aging,[4–7] and cancer.[8–12] One of the effects of DNA methylation is to physically impede the binding of transcription factors to their recognition sites, while the other is to bind proteins containing methyl-CpG-binding domains (MBDs),[13,14] which recruit additional proteins involved in the modification of chromatin. There are recent studies using DNA methylation as a tool for anticancer therapies with the goal of restoring normal DNA methylation patterns.[15]

The ability to detect the hypo-methylation or hyper-methylation state of the CpG sites is useful in predicting gene transcription, which can have profound consequences for human health. In a clinical setting, DNA methylation detection serves as a tool to screen at risk individuals for the early stages of cancer[16,17] and also evaluation after anticancer treatment.[18] All methods can be broadly divided into ensemble measurements and single-molecule measurements. The examples of the ensemble methods include methylation-specific polymerase chain reaction (PCR),[19] combined bisulfite restriction analysis (COBRA),[20] methylation-sensitive single-nucleotide primer extension (Ms-SNuPE),[21] methylated DNA immunoprecipitation,[22] hybridization arrays,[23–25] restriction landmark genome scanning,[26] next-generation sequencing after bisulfite conversion,[27] among others. These ensemble methods require a multitude of cells for analysis, with the apparent disadvantage that rare cells are poorly represented or have to be specifically enriched in order to make meaningful statements. That becomes particularly

[a)]Electronic mail: RRiehn@ncsu.edu.

important when the epigenetic state of small sub-populations such as cancer stem cells is sought. Further, clinically relevant haplotype and allele-specific mapping requires specialized additional steps.

In the field of protein biology, single-molecule investigations have yielded important insights into the intricate relationships of rare states in a population.[28] Single-molecule methylation detection has been recently demonstrated through nanopore technology[29] and single-molecule real-time (SMRT) DNA sequencing.[30] In principle, these methods require no front-end amplification and sample preparation of the DNA. Bisulfite conversion and sequencing schemes can also yield single-molecule data but cannot generally guarantee that single molecules were targeted and require intensive preparation.[31] All these techniques are capable of high throughput DNA methylation analysis at the level of the nucleotide bases with the capacity for parallel analysis.

However, the detection from single molecules is most meaningful when the methylome is derived from single cells, so that information about cell-cell variation can be derived. Since many cells need to be analyzed to gain statistical information, some of the above single-molecule analyses yield a flood of data, and thus data assembly becomes a significant barrier. Preparation steps are also difficult to integrate with single-cell analysis. We aim to provide a complimentary single-molecule technique that determines the methylation state with a lower resolution and minimal preparation, but from longer molecules, while maintaining spatial resolution. Since CpG islands close to promoter sites are the predominant target, we believe that a resolution somewhat better than the size of a single human gene is sufficient. In order to obtain haplotype data from single cells and to enable real-time data analysis without deep databases, we aim at analyzing DNA fragments that contain at least 100 kbp and up to a few Mbp.

In our work, methylation patterns are detected through binding of a fluorophore-tagged methyl-CpG-binding domain protein fragment to the interrogated dsDNA segment, as shown in Fig. 1. The binding pattern along the DNA is detected by fluorescence microscopy. In order to achieve single-gene relevant resolution, DNA is stretched by confinement to a quasi one-dimensional nanochannel (Fig. 2).[32] The technique is, thus, conceptually similar to fluorescence *in situ* hybridization on molecules that were enlongated molecules (fiber-FISH),[33] which are arrested in their extended configuration through a technique such as molecular combing.[34]

Nanochannel stretching itself is an emergent technique that has been used to map the length of DNA fragments,[32] image the binding of green fluorescent protein (GFP)-fusion transcription factors,[35] observe real-time ordered restriction mapping,[36] and perform single-molecule melting temperature mapping.[37] The capability for automated high-throughput mapping has been demonstrated.[38]

While nanochannel mapping appears similar to stretching through molecular combing, it differs in that the stretched state represents the equilibrium configuration of the molecule such that the molecule can fluctuate around that equilibrium configuration. In contrast, fiber-FISH and molecular combing lock the nucleic acid in a single non-equilibrium configuration.[39] Because of the inherent fluctuations, the resolution of a nanochannel experiment can be increased simply by extending the observation period of a single molecule, while a molecular combing/fiber-FISH experiment relies on measuring multiple independent molecules. The existence of the out-of equilibrium state in molecular combing and related stretching techniques accounts for the success of the molecular combing approach in restriction mapping where the axial tension is the basis of gap formation.[40] However, it is also the source of limitations in read length since the high tension needed for homogeneous stretching of long molecules tends to induce double-stranded breaks, which have to be compensated for by significant coverage and subsequent alignment of intermediate size reads[41] or construction of bacterial artificial chromosome (BAC) or phage artificial chromosome (PAC) libraries.[42] For that reason, researchers in the field have tended to lower the tension by using imperfect stretching, which leads to a decrease in the stretching homogeneity.[43] Thus, the fluorescence intensity of a dye adsorbed by the stretched molecule often serves as an indication of genomic length (instead of spatial location).

A further difference is in the nature of automation of the experiment. After a molecule is analyzed in a nanochannel, another molecule can be introduced into the same channel, and the

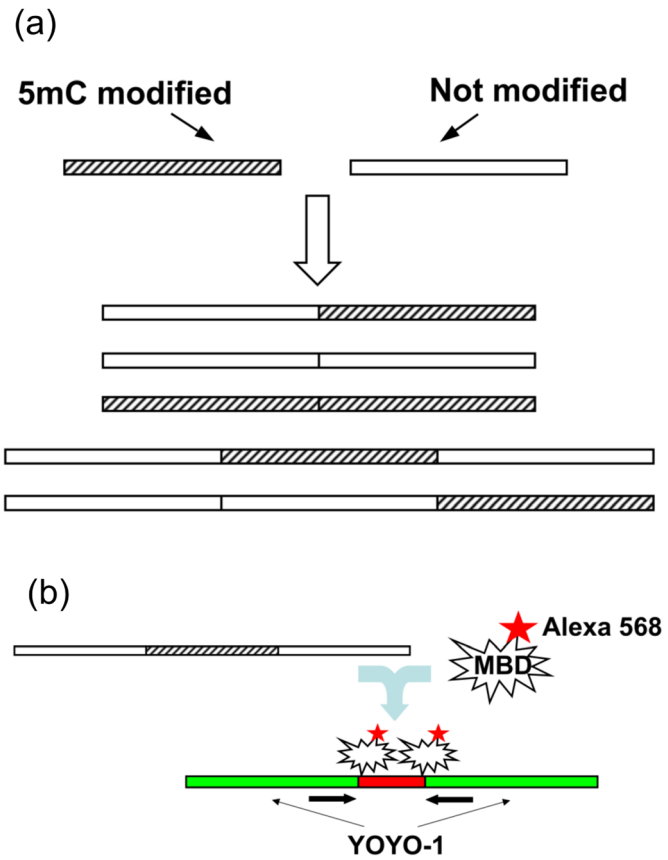

FIG. 1. (a) Schematic of possible outcomes of DNA concatemer formation with 5-cytosine methylated (5mC) and non-methylated segments. (b) Schematic of Alexa568-MBD to DNA concatemer. The entire molecule is stained using the green stain YOYO-1 and Alexa568-MBD binds to methylated stretches.

process can be repeated. Nanochannel devices can operate over multiple hours analyzing many molecules flowing through the device. In contrast, molecular combing surfaces are typically single-use, and so either a new substrate has to be used or multiple cells and chromosomes are

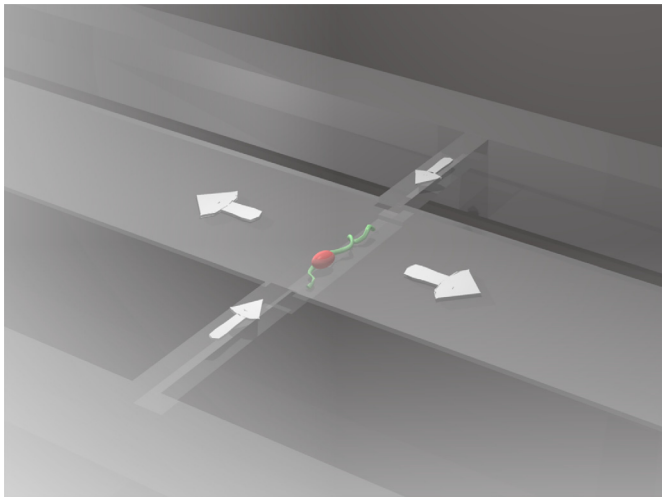

FIG. 2. Schematic of a device with two microchannel feeds (top and bottom) that are bridged by a nanochannel (inflowing arrows) containing an Alexa568-MBD labeled DNA concatemer. A shallow central shunt channel (outflowing arrows) allows the use of pressure-driven flow.

analyzed on a single surface. The main drawback of the nanochannel technique is the need for careful minimization of unspecific adhesion of the analyzed material to channel walls.

Our technique is very distinct from the recently published single-chromatin analysis at the nanoscale (SCAN).[44] These authors detect the methylation of DNA fragments in nanofluidic channels under flow and only demonstrated coincidence of fluorescent MBD and DNA. We demonstrate that the binding location within the molecule can be determined since our molecules are efficiently stretched out and can be observed over extended times.

In order to provide a robust testing vehicle with minimal biological complexity, we used λ-phage DNA concatemers as a model system for genomic DNA (Fig. 1). By concatenating fully CpG-methylated and non-methylated strands, we created a predictable barcode that enables us to judge both the detection efficacy and the mechanical properties of the probe-substrate complex. We have shown that MBD binds specifically to methylated DNA and that the spatial location of binding sites within the molecules can easily be mapped. However, we also noticed that binding of MBD to methylated DNA segments leads to a contraction that is dependent on the MBD quality. We believe that the success in using this artificial barcode sample implies that the technique can be extended to real genomic DNA molecules. Our results imply detection resolution on the order of 10 kbp, which is roughly the size of an average human gene.

II. MATERIALS AND METHODS

A. Preparation of essential biological materials

The vector, pET6HMBD (a gift from Sally H. Cross), was expressed in the *Escherichia coli* strain BL21 (DE3) pLysS, and MBD was purified using Ni-NTA agarose beads followed by FPLC with a monoQ column. Expression and purification were verified using SDS-PAGE.

About 0.38 mg of Alexa Fluor 568® (Invitrogen, called Alexa568 in the following) carboxylic acid and succinimidyl ester dye (first diluted in 2.5 μl of DMSO) were added to 360 μl of 84.6 μM of the purified MBD. The dye conjugation was performed at 4 °C on a rotating vial rack. Purification of the dye labeled MBD was performed on a sephadex G-50 column. Collected fractions were analyzed using UV-Vis, and the most efficiently conjugated fractions were reserved for use.

Methylation of λ-DNA was performed using CpG methyltransferase (M.SssI) from New England Biolabs (NEB) according to their standard protocol.

B. Controls

Controls using non-methylated and methylated λ-DNA were incubated against Alexa568 MBD to determine the specificity of the protein against the methylated binding sites. One μg each of non-methylated λ-DNA and methylated λ-DNA were incubated with a two-fold concentration of Alexa568 labeled MBD relative to the concentration of CpG sites in the DNA. The Alexa568-labeled MBD was first filtered through a 0.03 μm polycarbonate membrane using an Avanti mini-extruder before use. The DNA and MBD were incubated at 37 °C for 4 h in the dark, followed by quenching to 4 °C in preparation for dialysis. Excess MBD was dialyzed in a genomic tube-o-dialyzer (G-Biosciences) at 4 °C overnight in 1/2 TBE buffer, *p*H 8, with added 0.1% Tween® 20 and 2 mM β-mercaptoethanol.

C. DNA concatemer formation and staining

Once assured of the specificity by the control tests, non-methylated and methylated λ-DNA were assembled at a 1:1 ratio by annealing at 72 °C briefly and then slowly cooling to 4 °C. A mixture of concatemers was obtained, with shorter length concatemers occurring at higher frequency than the longer length ones.

Alexa568-labeled MBD was first filtered through a 0.03 μm polycarbonate membrane using a mini-extruder (Avanti Polar Lipids) before use. A three-fold concentration of Alexa568 labeled MBD relative to the concentration of CpG sites in the DNA was reacted with 2 μg of barcode DNA at 37 °C for 4 h in the dark, followed by rapid cooling to 4 °C. Excess MBD was

dialyzed as above in the dark. Alexa568 labeled DNA is counter stained with the intercalating dye YOYO-1 (Invitrogen) at a ratio of 1 dye molecule per 50 base pairs of DNA. YOYO-1 dye has emission sufficiently distinct from Alexa568, and when adjusted for concentration, it can be imaged at comparable intensity to Alexa568.

In the final imaging solution, a 0.1 μm filtered 10 kDa MW PVP is used at 1% by weight, and the concentrations of DTT and PMSF adjusted to 5 mM and 0.5 mM, respectively. The concentration of the concatenated DNA during imaging is roughly 1 μg/ml.

D. Operational procedure of observation

Integrated nano/microfluidic channels were fabricated in fused silica using methods described elsewhere.[45] The device layout is illustrated in Fig. 2, following a design principle demonstrated by Reisner *et al.*,[37] in which DNA is localized in the field of view through the combination of nanogrooves and a thin shunt layer that allows liquid to escape but traps DNA within the grooves. Note that the actual device is an array of such channels. The effective channel cross-section was 250×200 nm^2, and the shunt channel was 50 nm deep. Channel dimensions were confirmed using SEM after the device had been used in experiments.

DNA was driven through both microfluidic and nanofluidic channels using total pressures of about 30 psi. Once molecules had been localized, the pressure was removed to recover an equilibrium configuration that is independent of liquid flow. After observation the channels were flushed using one-sided pressure application.

Molecules were observed using an inverted fluorescence microscope with a 100x, 1.35 N.A. oil immersion objective (Nikon) coupled to an em-CCD (Andor). Simultaneous dual channel imaging of the green and red images is enabled by a DV2 Beam Splitter (MAG Biosystems), where the red channel is centered at 620/60 and the green channel at 520/40. Green and red images were obtained under illumination from 473 and 561 nm DPSS lasers, respectively, with no detectable contamination of the green channel by Alexa568 or the red channel by YOYO-1.

III. RESULTS AND DISCUSSION

We tested false positive and false negative rates by incubating Alexa568-MBD with fully methylated and non-methylated DNA samples containing mostly λ-DNA monomers and half-mers. The latter is consistently present in commercial DNA samples and can constitute half of all molecules. With non-methylated DNA we found an abundance of freely drifting YOYO-1 stained DNA coils, no Alexa568/YOYO-1 co-localization events and a dim, fairly homogenous Alexa568 background. The same experiment with methylated DNA yielded a vastly reduced number of YOYO-1 stained DNA coils (1% of expected), a high rate of co-localization, and a Alexa568 signal characterized by compact globules that had adhered to the glass substrate. By counting each molecule as one event, we quantified the false positive rate as less than 1% and the false negative rate as less than 0.6%.

The apparent compaction of DNA molecules upon MBD binding is in all probability due to self-interaction of MBD and is not present for methylated DNA in the absence of MBD. We note that this aggregation tendency increases with storage time or freeze-thaw cycles and that it may be accelerated by the limited solubility of Alexa568 fluorophore. Best results were obtained using MBD that was used within 1 week of MBD expression. The apparent competitive binding between YOYO-1 and Alexa568-MBD is likely due to a barrier to binding that is imposed by the formation of a tight DNA globule when MBD aggregates.

We then introduced DNA into nanochannel devices, as described in Sec. II. We observe binding patterns as predicted by the random design of the DNA substrate. Fig. 3 shows a collection of observed fluorescence patterns from molecules incorporating MBD-labeled stretches. MBD-binding occurred in continuous stretches, and not as dots along a line. Each λ-monomer has about 3000 CpG sites. Fig. 3(a) shows an λ-DNA trimer where the central monomer is methylated. A trimer with a terminal methylated monomer is shown in Fig. 3(b). A heterodimer is shown in Fig. 3(c). In all panels we note that both DNA and MBD are co-localized and

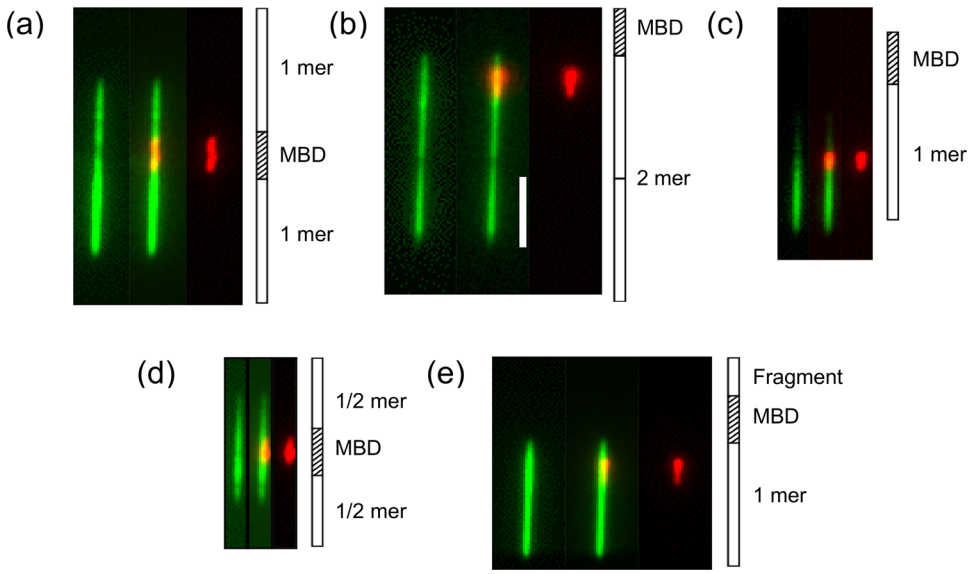

FIG. 3. (a) Fluorescence images of concatenated methylated and non-methylated λ-DNA labeled with Alexa568MBD (red) and YOYO-1 (green), stretched out in nanochannels. Within each panel colors are split for clarity; (left) YOYO-1 only (DNA), (center) composite, (right) Alexa568 only (Alexa568-MBD). Schematic drawings in each panel illustrate the spatial position of the Alexa Fluor 568 MBD and the length of the λ-DNA. The scale bar in panel (b) is 5 microns.

stretched out. However, we typically observed that the length of a MBD-conjugated methylated λ-monomer is roughly a quarter to a third of that of a fully extended lambda monomer. This shortening upon MBD binding is attributable to the same MBD self-interaction that we reported for our controls. Tests on pure methylated DNA showed that methylation does not influence the mechanical properties in channels, at least on the scale seen when bound to MBD. Self-interaction also appeared to increase with the age of the Alexa568-MBD construct. A considerable fraction of molecules showed patterns indicating that the concatenation was terminated by halfmers, which is expected. For instance, Fig. 3(d) shows a methylated monomer flanked by two non-methylated halfmers. In some cases, even shorter fragments are present, such as in Fig. 3(e), although a small probability exists that the MBD could have been mechanically stripped from one end upon insertion into the nanochannel.

We determined the length of the molecule and the MBD binding position by fitting of Gaussian-widened boxcar functions to both the red and green channels for each frame and then determined averages of all parameters for each molecule. Because of the large number of possible combinations of methylated and unmethylated monomers and halfmers, a global statistical analysis of binding locations and concatenation patterns was not feasible with the number of molecules in our study. We, thus, based our statistical analysis of the binding location on a subset of molecules containing MBD binding events for which the total length of the analyzed molecule fell within one of the main peaks of the length histogram. That length coincides with a length that we attribute to the combination of a heterodimer containing both methylated and unmethylated stretches. A histogram charting the ratio of the distance between the center of the MBD signal and the end of the molecule closest to the MBD is shown in Fig. 4. The determination of an absolute position is not possible since DNA can thread into the channel with either end. The consensus location of about 0.2 is expected for molecules in which the MBD-conjugated methylated DNA segment is contracted to about one quarter of its bare length. The spread in binding locations is likely due to the presence of sheared DNA (especially methylated halfmers), variations in the quality of the MBD leading to increased aggregation, and perhaps partial stripping of the MBD during violent nanochannel insertion events.

We can estimate the resolution of our technique from the extension of partially stretched MBD domains. We have observed that MBD-bound methylated λ-DNA monomers of 48.5 kbp length consistently stretch to a length of 1.3 microns. Since the resolution of our technique is

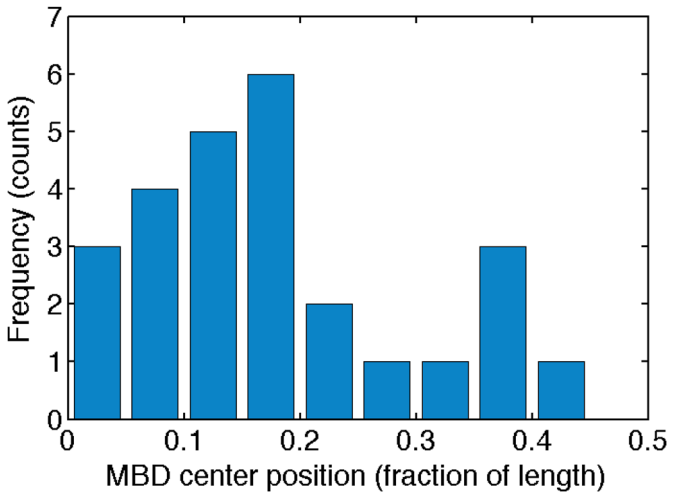

FIG. 4. Histogram of MBD center positions for total DNA lengths of 3 ± 0.5 microns. The spread in binding position in largely due to the spread in substrate lengths.

approximately given by the diffraction limit, that would correspond to a resolution of about 10 kbp, which is comparable to the size of a human gene. Hence, we believe that our technique is applicable to gene specific mapping of hyper-methylated and hypo-methylated sites on genomic DNA.

The major impediment of the achievable resolution is the aggregation tendency of the MBD. This can likely be overcome through careful optimization of the fluorescent MBD construct. In particular, a wide screening for more suitable dyes and point mutations of non-essential amino acids are strategies with a probability of success. Further potential enhancements of the resolution and stretching of the MBD coupled segments are adjusting the types of buffer, buffer *p*H, salt concentration, and additives. Reduced self-aggregation, coupled with smaller channel widths, will result in higher overall stretching ratios. While no fundamental limitations to resolution exist, we note that at 1 kbp, the resolution of DNA sizing in nanochannels is a likely limit.

IV. CONCLUSIONS

In conclusion, we present a technique for the mapping of 5-methyl cytosine modification of CpG clusters in genomic length DNA with a resolution of about 10 kbp. We have demonstrated low false positive and negative rates and have shown methylation patterns consistent with a prepared barcode pattern. We believe that the technique will be capable to derive gene-relevant data from single molecules.

ACKNOWLEDGMENTS

We acknowledge funding from the National Institutes of Health (Grant Nos. R21CA132075 and R21HD065222). A portion of this research was conducted at the Center for Nanophase Materials Sciences, which is sponsored at Oak Ridge National Laboratory by the Scientific User Facilities Division, US Department of Energy. This work was performed in part at the Cornell NanoScale Facility, a member of the National Nanotechnology Infrastructure Network, which is supported by the National Science Foundation (Grant No. ECS-0335765). T.A.L. was supported through NSF Award No. 0353719.

[1]Z. Siegfried and H. Cedar, Curr. Biol. **7**, R305 (1997).
[2]K. D. Robertson and P. A. Jones, Carcinogenesis, **21**, 461 (2000).
[3]A. Bird, Genes Dev. **16**, 6 (2002).
[4]A. C. Ferguson-Smith and M. A. Surani, Science **293**, 1086 (2001).

[5]E. Li, C. Beard, and R. Jaenisch, Nature **366**, 362 (1993).
[6]J. T. Lee, Curr. Biol. **13**, R242 (2003).
[7]K. D. Robertson, Nat. Rev. Genet. **6**, 597 (2005).
[8]P. A. Jones and P. W. Laird, Nat. Genet. **21**, 163 (1999).
[9]S. B. Baylin and J. G. Herman, Trends Genet. **16**, 168 (2000).
[10]B. A. Ponder, Nature **411**, 336 (2001).
[11]J.-P. Issa, Clin. Immunol. **109**, 103 (2003).
[12]S. B. Baylin and J. E. Ohm, Nat. Rev. Cancer **6**, 107 (2006).
[13]X. Nan, R. R. Meehan, and A. Bird, Nucleic Acids Res. **21**, 4886 (1993).
[14]S. H. Cross, J. A. Charlton, X. Nan, and A. P. Bird, Nat. Genet. **6**, 236 (1994).
[15]X. Yang, F. Lay, H. Han, and P. A. Jones, Trends Pharmacol. Sci. **31**, 536 (2010).
[16]P. A. Jones, S. B. Baylin, and S. Kimmel, Nat. Rev. Genet. **3**, 415 (2002).
[17]S. A. Belinsky, Nat. Rev. Cancer **4**, 707 (2004).
[18]P. Wijermans, M. Lübbert, G. Verhoef, A. Bosly, C. Ravoet, M. Andre, and A. Ferrant, J. Clin. Oncol. **18**, 956 (2000).
[19]M. F. Fraga and M. Esteller, Biotechniques **33**, 632 (2002).
[20]Z. Xiong and P. W. Laird, Nucleic Acids Res. **25**, 2532 (1997).
[21]M. L. Gonzalgo and G. Liang, Nat. Protoc. **2**, 1931 (2007).
[22]M. Weber, J. J. Davies, D. Wittig, E. J. Oakeley, M. Haase, W. L. Lam, and D. Schübeler, Nat. Genet. **37**, 853 (2005).
[23]M. Bibikova, Z. Lin, L. Zhou, E. Chudin, E. W. Garcia, B. Wu, D. Doucet, N. J. Thomas, Y. Wang, E. Vollmer, T. Goldmann, C. Seifart, W. Jiang, D. L. Barker, M. S. Chee, J. Floros, and J.-B. Fan, Genome Res. **16**, 383 (2006).
[24]P. S. Yan, D. Potter, D. E. Deatherage, S. Lin, and T. H.-M. Huang, in *DNA Methylation: Methods and Protocols*, Methods in Molecular Biology Vol. 507, 2nd ed., edited by J. Tost (Humana, Totowa, NJ, 2009), Chap. 8, pp. 89–106.
[25]S. Nautiyal, V. E. H. Carlton, Y. Lu, J. S. Ireland, D. Flaucher, M. Moorhead, J. W. Gray, P. Spellman, M. Mindrinos, P. Berg, and M. Faham, Proc. Natl. Acad. Sci. **107**, 12587 (2010).
[26]Y. Ando and Y. Hayashizaki, Nat. Protoc. **1**, 2774 (2006).
[27]S. J. Cokus, S. Feng, X. Zhang, Z. Chen, B. Merriman, C. D. Haudenschild, S. Pradhan, S. F. Nelson, M. Pellegrini, and S. E. Jacobsen, Nature **452**, 215 (2008).
[28]S. Weiss, Science **283**, 1676 (1999).
[29]J. Clarke, H.-C. Wu, L. Jayasinghe, A. Patel, S. Reid, and H. Bayley, Nat. Nanotechnol. **4**, 265 (2009).
[30]B. A. Flusberg, D. R. Webster, J. H. Lee, K. J. Travers, E. C. Olivares, T. A. Clark, J. Korlach, and S. W. Turner, Nat. Methods **7**, 461 (2010).
[31]E. Hodges, A. D. Smith, J. Kendall, Z. Xuan, K. Ravi, M. Rooks, M. Q. Zhang, K. Ye, A. Bhattacharjee, L. Brizuela, W. R. McCombie, M. Wigler, G. J. Hannon, and J. B. Hicks, Genome Res. **19**, 1593 (2009).
[32]J. O. Tegenfeldt, C. Prinz, H. Cao, S. Chou, W. W. Reisner, R. Riehn, Y. M. Wang, E. C. Cox, J. C. Sturm, P. Silberzan, and R. H. Austin, Proc. Natl. Acad. Sci. USA **101**, 10979 (2004).
[33]H. H. Q. Heng, J. Squire, and L. C. Tsui, Proc. Natl. Acad. Sci. USA **89**, 9509 (1992).
[34]A. Bensimon, A. Simon, A. Chiffaudel, V. Croquette, F. Heslot, and D. Bensimon, Science **265**, 2096 (1994).
[35]Y. M. Wang, J. O. Tegenfeldt, W. Reisner, R. Riehn, X. J. Guan, L. Guo, I. Golding, E. C. Cox, J. Sturm, and R. H. Austin, Proc. Natl. Acad. Sci. USA **102**, 9796 (2005).
[36]R. Riehn, M. C. Lu, Y. M. Wang, S. F. Lim, E. C. Cox, and R. H. Austin, Proc. Natl. Acad. Sci. USA **102**, 10012 (2005).
[37]W. Reisner, N. Larsen, A. Silahtaroglu, A. Kristensen, N. Tommerup, J. Tegenfeldt, and H. Flyvbjerg, Proc. Natl. Acad. Sci. USA **107**, 13294 (2010).
[38]C. H. Reccius, S. M. Stavis, J. T. Mannion, L. P. Walker, and H. G. Craighead, Biophys. J. **95**, 273 (2008).
[39]C. Schurra and A. Bensimon, Methods Mol. Biol. **464**, 71 (2009).
[40]D. C. Schwartz, X. Li, L. I. Hernandez, S. P. Ramnarain, E. J. Huff, and Y. K. Wang, Science **262**, 110 (1993).
[41]A. Valouev, D. C. Schwartz, S. Zhou, and M. S. Waterman, Proc. Natl. Acad. Sci. USA **103**, 15770 (2006).
[42]X. Michalet, R. Ekong, F. Fougerousse, S. Rousseaux, C. Schurra, N. Hornigold, M. van Slegtenhorst, J. Wolfe, S. Povey, J. S. Beckmann, A. Bensimon, Science **277**, 1518 (1997).
[43]E. T. Dimalanta, A. Lim, R. Runnheim, C. Lamers, D. K. Churas, A. Forrest, J. J. de Pablo, M. D. Graham, S. N. Coppersmith, S. Goldstein, D. C. Schwartz, Anal. Chem. **76**, 52935301 (2004).
[44]B. R. Cipriany, R. Zhao, P. J. Murphy, S. L. Levy, C. P. Tan, H. G. Craighead, and P. D. Soloway, Anal. Chem. **82**, 2480 (2010).
[45]R. Riehn, W. Reisner, J. O. Tegenfeldt, Y. M. Wang, C.-K. Tung, S. F. Lim, E. C. Cox, J. Sturm, and R. H. Austin, *Integrated Biochips for DNA Analysis*, 1st ed., edited by R. H. Liu and A. P. Lee (Landes Bioscience, Austin, Texas, 2007), Chap. 12, pp. 151–186.